 SL, vol.3, no.1, pp.1-36, 2010

Application of Advanced Mechanics for the Structural Design of Sodium Cooled Fast Reactor Components

P. Chellapandi[1], S.C. Chetal[1] and Baldev Raj[1]

Abstract: Some of the safety critical components of sodium-cooled fast reactors (SFR) are large dimensioned thin-walled shell structures. These components hold a large sodium mass and are subjected to high temperatures (820 K), high temperature gradients and cyclic thermal loads. The components are designed for long design life (>40 y). These features introduce complicated cyclic thermo-plastic deformations, the need for applying the principles of fracture mechanics under high cycle thermal fatigue, structural instabilities, fluid-structure interactions including elastic instabilities and high strain rate deformations. Hence, the structural design of such components is performed by addressing the relevant concepts in mechanics. In this paper, results of application of such advanced concepts for the structural design of components of the 500 MWe Prototype Fast Breeder Reactor (PFBR), which is under construction at Kalpakkam, are highlighted. New rules are recommended for inclusion in design codes like RCC-MR.

1 Introduction

In India, a 500 MWe Prototype Fast Breeder Reactor (PFBR) is in an advanced stage of construction at Kalpakkam. The reactor is scheduled to be commissioned by 2012. PFBR is a sodium-cooled pool type reactor with 2 primary and 2 secondary loops with 4 steam generators per loop. The overall flow diagram comprising the primary circuit housed in the reactor assembly, the secondary sodium circuit and the balance of plant is shown in Fig. 1. The nuclear heat generated in the core (1250 MWt) is removed by circulating sodium from the cold pool at 670 K to the hot pool at 820 K. The sodium from the hot pool after transporting its heat to four intermediate heat exchangers (IHX) mixes with the cold pool. The circulation of sodium from the cold pool to the hot pool is maintained by two primary sodium pumps and the flow of sodium through the IHXs is driven by a level difference (1.5 m of sodium) between the hot and cold pools. The heat from IHXs is in turn trans-

[1] Indira Gandhi Centre for Atomic Research, Kalpakkam-603 102

ported to eight steam generators (SG) by sodium flowing in the secondary circuit. Steam produced in the SGs is supplied to a turbo-generator to produce 500 MWe.

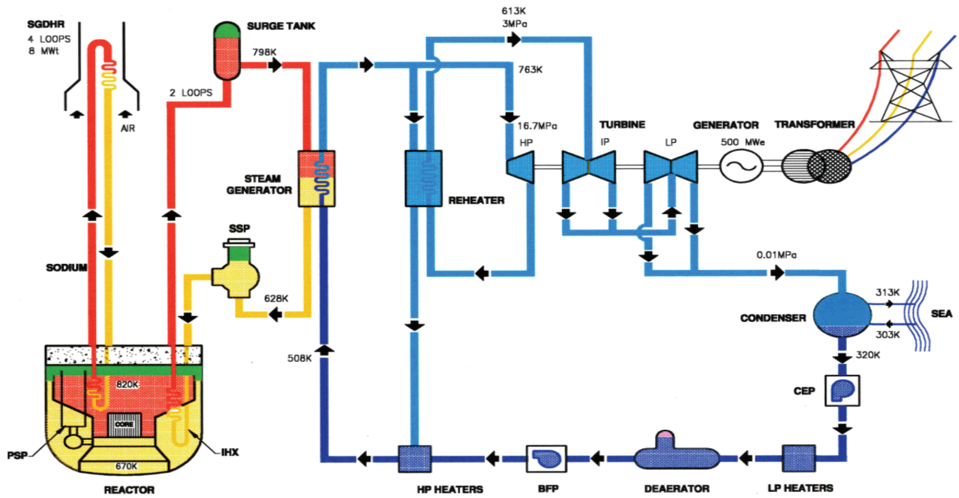

Figure 1: PFBR flow sheet

In the reactor assembly (Fig. 2), the main vessel houses the entire primary sodium circuit including the core. The sodium is filled in the main vessel with the free surface blanketed by argon. The inner vessel separates the hot and cold sodium pools. The reactor core consists of 1757 subassemblies including 181 fuel subassemblies. The control plug, positioned just above the core, houses 12 absorber rod drive mechanisms. The top shield supports the primary sodium pumps, the IHX, the control plug and the fuel handling systems. PFBR uses a mixed oxide with natural uranium and approximately 30 % Pu oxide as fuel. For the core components, 20 % cold worked D9 material (15 % Cr- 15 % Ni with Ti and Mo) is used to have better irradiation resistance. Austenitic stainless steel type 316 LN is the main structural material for the out-of-core components and modified 9Cr-1Mo (grade 91) is chosen for the SGs. The PFBR is designed for a plant life of 40 y with a load factor of 75 %.

In the design of PFBR components, many challenging aspects have been addressed comprehensively [Baldev Raj (2008)]. A few of them are high temperature design for long reliable operation of components operating at temperatures around 820 K for a design life of 40 years, design of mechanisms and rotating equipment operating in sodium and argon cover gas space, handling sodium leaks and sodium water reactions in the SG, seismic analysis of interconnected buildings resting on

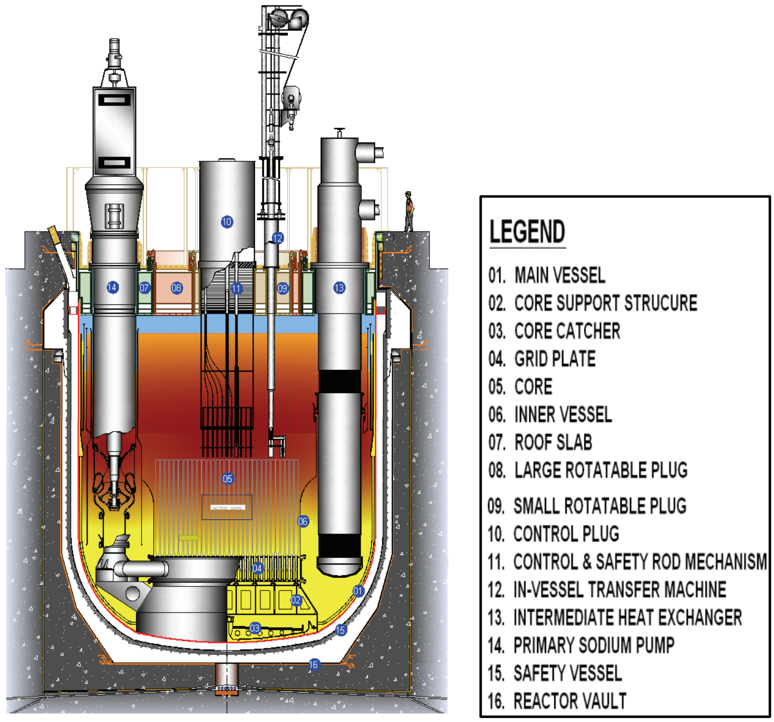

Figure 2: Schematic sketch of PFBR reactor assembly components

the common base raft, seismic design of thin walled vessels, pumps and absorber rod mechanisms and in-service inspection of reactor internals within sodium. The design is carried out comprehensively addressing all the possible failure modes as shown in Fig. 3 [Chellapandi, Chetal and Baldev Raj (2009)].

Sodium coolant remains in the liquid state up to 950^{o}C and hence there is no need of pressurisation. The operating pressure for the components except the grid plate along with primary sodium pipes is due to the hydrostatic head of sodium. The grid plate contains sodium at a pressure of 0.8 MPa required to pump the sodium through the core subassemblies overcoming high pressure drops. Similarly, the steam generator tubes operate at 17 MPa on the steam side. The induced stress due to pressure on the sodium components is insignificant. In view of the hot and cold pools co-existing in the reactor assembly, the operating temperature can vary from 670 K to 820 K. This large temperature difference in sodium imposes a high ΔT on the structural wall during normal and transient conditions. Thus, a few special

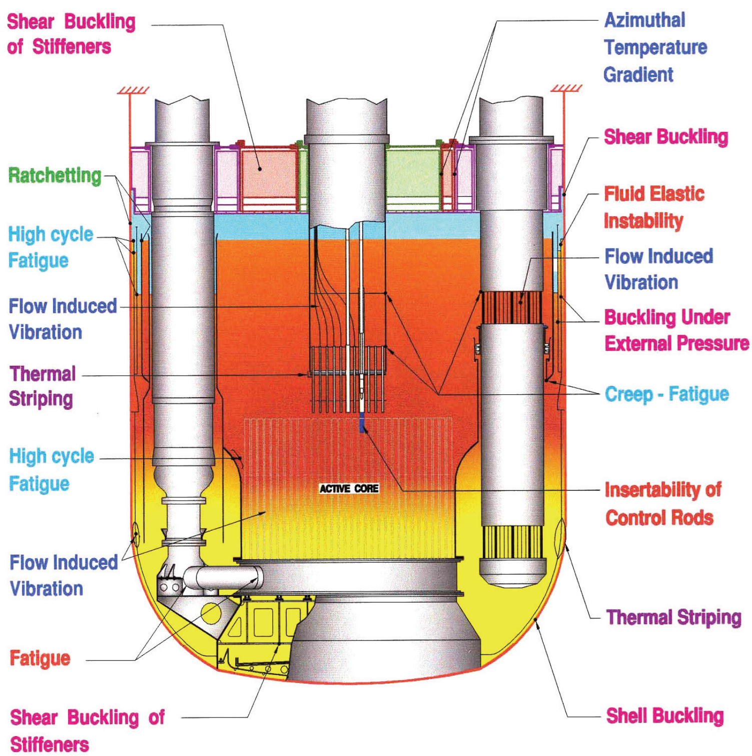

Figure 3: Failure modes for structural design

structural failure modes are induced by thermal loads and their thermo-mechanical effects. In order to accommodate thermal expansions without introducing high thermal stresses, the structural members should be flexible and have only the minimum necessary wall thickness. Hence, SFR structures operating in sodium are generally thin walled shells. This also has high economic advantages with respect to material consumption. To meet the requirement of high temperatures and temperature variations, most of the vessels containing sodium are fixed at the top, allowing free expansion in the downward direction. Further, there are many coaxial shells, such as the main vessel, thermal baffles and the inner vessel with a narrow annular space confining sodium. Such structural features, i.e. large size vessels supported at one end carrying a large sodium mass and the presence of narrow annular gaps filled with sodium, generate maximum dynamic amplification during a seismic event. Buckling of thin shells under the seismic forces decide their structural wall thickness. Since, the components are designed for a long life (40-60 y) and high load factors (75-90 %), time dependent failure modes due to creep effects are dominant. These decide the life of the components.

In this paper, design approach adopted for reactor assembly components of PFBR, advanced mechanics concepts applied to analyse a few specialized failure modes specific to SFR and some sample analysis results are highlighted. Further, new structural design rules are recommended for consideration in future versions of RCC-MR.

2 PFBR design approach

Robust and proven design concepts are considered giving due consideration to operating experience of SFR worldwide ($\sim$400 r-y). New concepts and materials introduced in PFBR for the first time in reactor design and mechanisms operating in sodium were thoroughly validated. The mechanical design and construction of components is carried out to comply with the rules of French code RCC-MR: 2002 [AFCEN, 2002]. As per this code, the design calls for detailed analysis using computer codes, which have undergone extensive validation exercise. Structural integrity assessment of components and systems subjected to extreme loading, in particular seismic and core disruptive accident loadings is ensured by testing and evaluation through appropriate simulated methodologies. In the first level, analysis is carried out assuming that the structures are free of any unacceptable defects. In the second level, severe violation of manufacturing and inspection specifications is assumed and analysis is carried out on the structures with postulated surface defects. In the third level, propagation of undetected cracks resulting in through wall propagation is assumed and subsequently ensured that such defects can be detected well in advance before they result in catastrophic failures such as complete loss of load carrying capacity (collapse). Towards this, the concept of leak before break is applied as per the guidelines recommended in RCC-MR: Appendix-A16 [AFCEN (2002)]. In these analyses carried out under these three levels, many advanced and interesting applied mechanics concepts are applied through extensive, analytical, numerical and experimental simulation techniques. Numerical stress analysis is performed using the finite element computer code called 'CAST3M' issued by CEA, France [CAST3M – User Manual (2003)].

3 Applicable advanced concepts of mechanics

Towards accurately predicting the life of components, viscoplastic models are generated with thorough understanding of mechanical behaviour of materials at high temperature under combined mechanical and cyclic thermal loads. Important phenomena to be simulated numerically are cyclic hardening and softening, progressive strain growth (thermal ratcheting) and progressive buckling. The thin shell structures under fluid induced forces are investigated for various instabilities, viz. liquid jet instability i.e thermal striping, fluid-elastic instability, parametric instability and elasto-plastic instability, i.e. buckling. Non-linear contact mechanics principles are applied for determining (i) dynamic displacements of core subassemblies, absorber rods and drive mechanisms and (ii) pump seizure behaviour under seismic induced forces. Advanced concepts of fracture mechanics are applied to (i) surface crack growth studies under cyclic thermal stresses (ii) for estimating the collapse of structures with defects (interaction of plasticity, tearing and buckling), (iii) fast transient fluid-structure interactions under core disruptive accident conditions, (iv) high strain & high strain rate loading effects on thin walled welded shell structures and (v) effects of manufacturing defects (form tolerances, weld defects) on structural integrity. Experimental mechanics are applied for simulation of instabilities and quantifications, monitoring of crack initiation and growth in the component models at high temperature, capturing of high strain rate strains and displacements.

4 Highlights of analysis

4.1 Deformation mechanics of components subjected to moving sodium free levels

Structures subjected to cyclic loads undergo complicated deformation behavior. This is basically due to material behavior under cyclic loads. The ultimate deformation behavior of the structures is the combined effects of material behavior and structural response to respect the continuity and equilibrium equations. Fig. 4 depicts the stress/strain cycling of material without any progressive plastic strain growth (Fig. 4a) as well as ratcheting, i.e. stress/strain cycling with incremental strain growth (Fig. 4b). The incremental strain growth would stabilize after a few number of cycles. The cumulative strain growth, however, should be limited to respect the strain limits specified in the design codes, for example 1 % for membrane strain and 2 % for bending strain across the wall thickness.

4.1.1 Ratcheting assessment of main vessel

In SFR, the main vessel, subjected to cyclic variation of axial temperature gradients in the vicinity of sodium free surface, accompanied with the steady mechanical load due to its self weight along with core, internals and sodium, undergoes ratcheting (Fig. 5). The deformation on the main vessel should be limited with respect to functional and structural integrity considerations. The most challenging aspect is the development of constitutive material model which can numerically simulate the

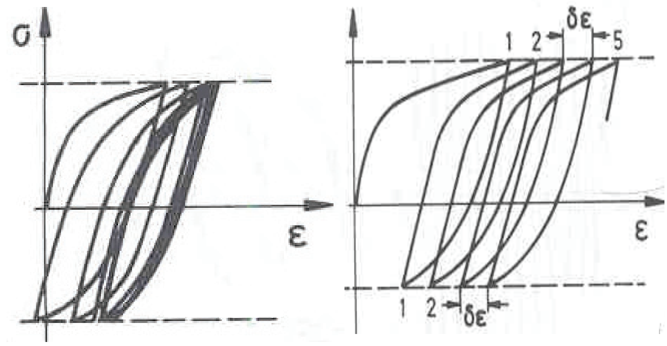

a **b**

Figure 4: Cyclic stress-strain behaviour material

ratcheting. Towards this, 'Reduced Chaboche Model' has been developed based on viscoplastic theory and implemented in the finite element code 'CONE' [Chellapandi and Alwar (1993)]. The ability of the code in predicting the complicated cyclic stress and strain behavior of stainless steel type SS 316 LN at 873 K is depicted in Fig. 6. Thermal ratcheting of main vessel has been predicted numerically with CONE code and demonstrated that the deformation is less than the allowable value of 15 mm [Chellapandi, Chetal and Bhoje (2000)]. Fig. 7 shows the details. The same has been validated by simulated experiments (Fig. 8).

4.1.2 Establishing acceptable reactor startup rate

In SFR, the reactor should be started up sufficiently slow so that induced strains and stresses shall be acceptable with respect to strain limits and cumulative creep-fatigue damage. Rising of levels in association with temperature raise causes high local deformations and stresses, which decide the rate of power rising from shut down. Reactor assembly components in the sodium pools are analysed comprehensively to quantify the effects at various startup rates and based on which the startup duration of 20 h is recommended [Suresh Kumar, Chellapandi and Chetal (2003)]. Fig. 9 shows typical results of analysis carried out for primary sodium pump shell in the vicinity of sodium free level.

4.2 Creep-fatigue damage assessment

In SFR, the design life of components is dictated by the accumulated creep-fatigue damage. Towards recommending the design life along with load factor for PFBR,

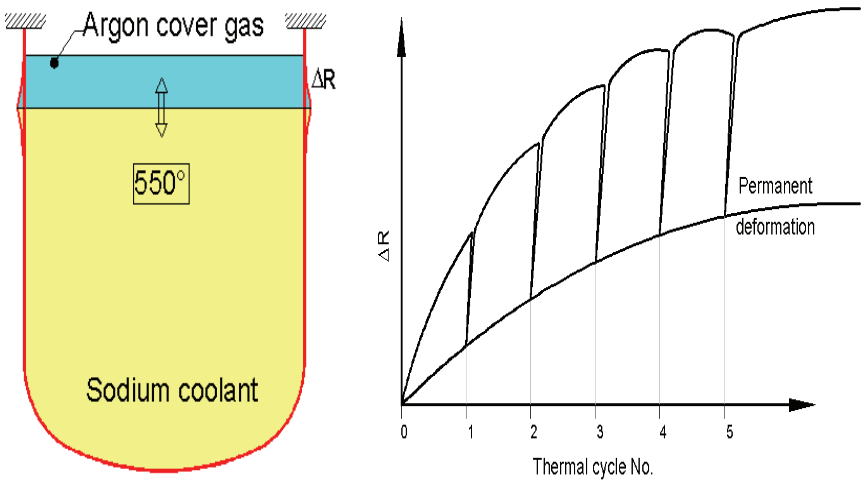

Figure 5: Ratchetting of main vessel near sodium free level

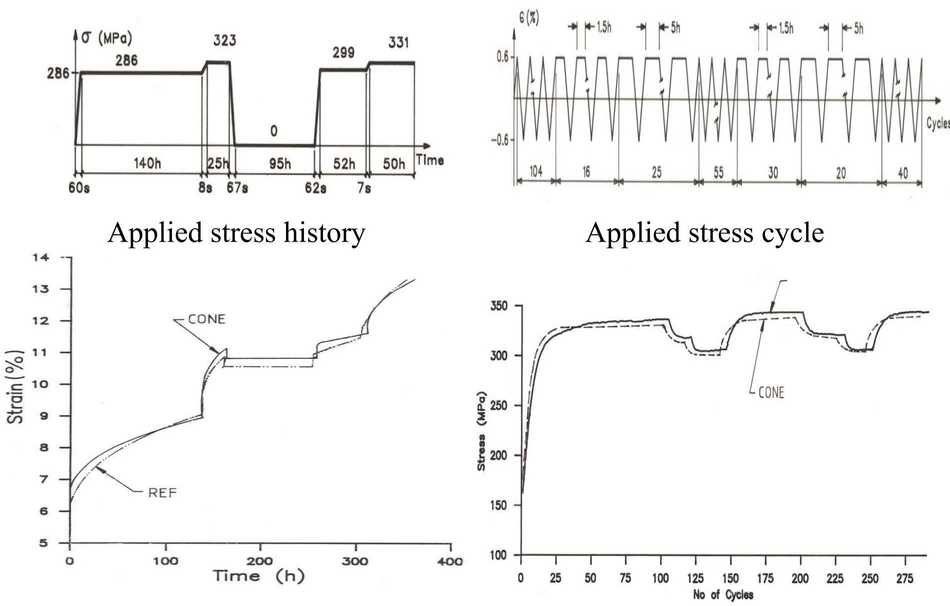

Figure 6: Cyclic viscoplastic stress strain behaviour of SS 316 LN at 873 K

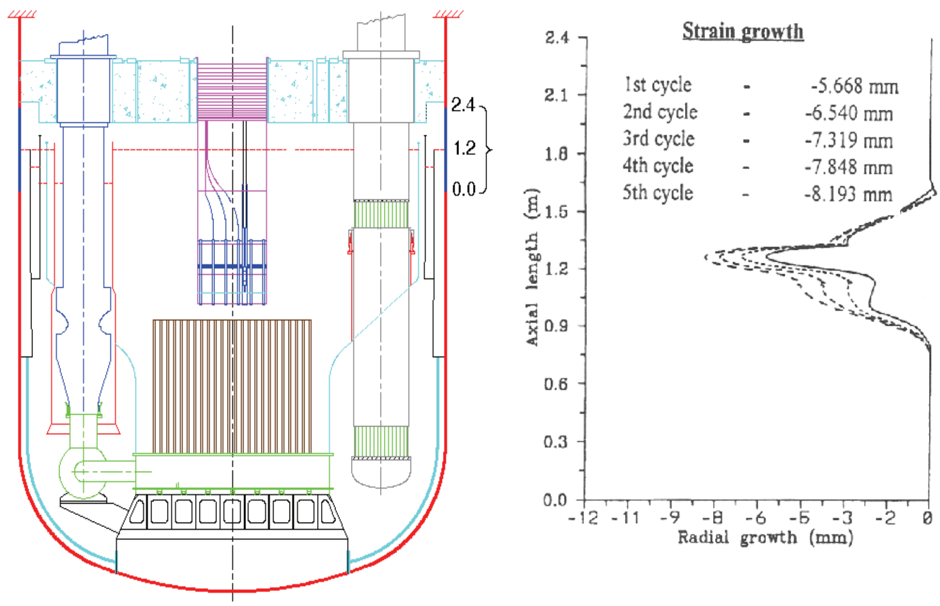

Figure 7: Ratcheting of main vessel

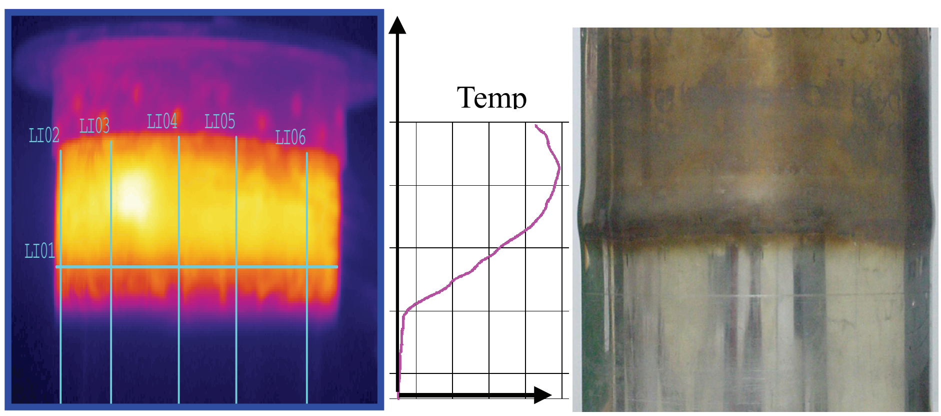

Figure 8: Experimental simulation of ratcheting

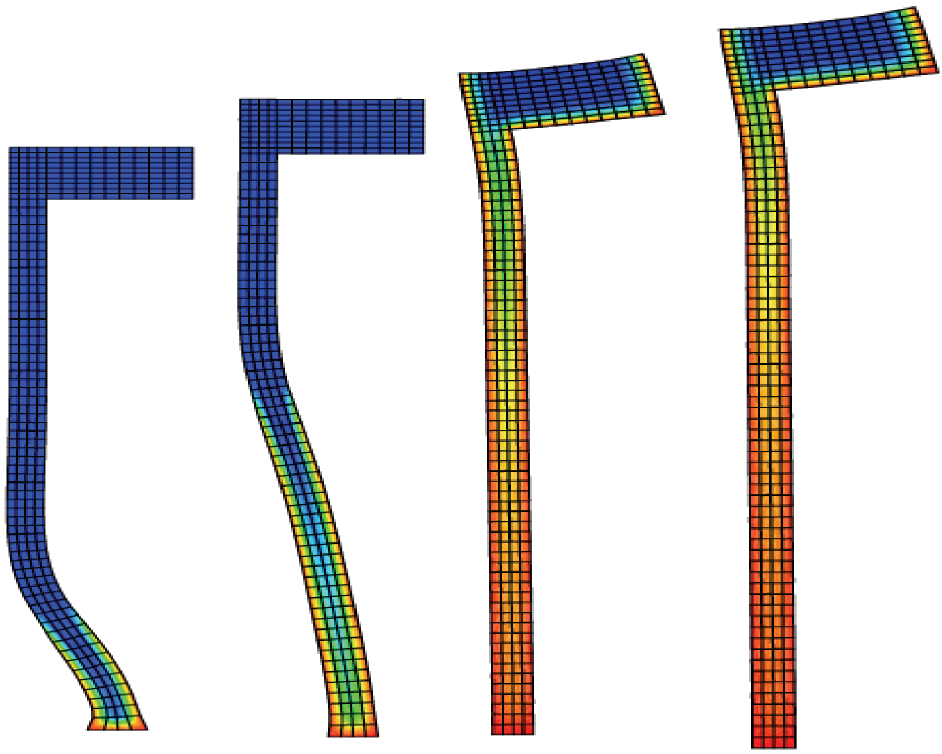

Figure 9: Evolution of temperature and deformations in pump shell in the vicinity of flange

reactor components are analysed in detail employing viscoplastic constitutive models. While the analysis has yielded realistic results, they also help to quantify the conservatism that has been incorporated in the simplified analysis procedure recommended in RCC-MR: 2002. A benchmark study was carried out for estimating the life of control plug junction under an idealized pessimistic thermal shock and the allowable creep-fatigue damage lives were estimated employing Chaboche viscoplastic constitutive model as well as simplified method [Chellapandi, Bhoje and Alwar (1996)]. The exercise indicates that the simplified analysis has conservatism up to a factor of ~ 5, compared to the realistic prediction, as seen in Tab. 1, which shows the allowable number of scrams.

Table 1: Allowable load cycles for control plug

Analysis method	Operating temperature - K		
	805	815	825
RCC-MR:2002: Simplified method	51	17	10
RCC-MR:2002: Viscoplastic analysis	132	82	53

The analysis has been validated through simulated tests on simplified geometries, having component features such as multiaxiality, stress concentrations and welds. Fig. 10 depicts the experimental benchmark, which brings out the conservatism on the life estimated using simplified methodologies recommended in RCC-MR: 2002 and 2007 editions.

4.3 Life prediction of components with defect

The nuclear codes specify stringent inspection requirements to ensure high quality of structural materials and manufacturing standards. In view of the fact that welds are weak links in a structure, the codes do not permit welds without adequate and reliable inspection methodologies. Accordingly, the design procedures presented in the above paragraphs are applicable for the welds having no deviations that are unacceptable by the design codes. However, in practical situations, a few difficult locations in the form of crack-like defects, termed 'geometrical singular points' are unavoidable. For such welded structures with crack like defects, RCC-MR provides special rules based on'σ_d approach' in annexure A16. As per this procedure, the creep and fatigue damage accumulated till the end of the design life is calculated at the characteristic distance 'd' from the crack tip and should satisfy the creep-fatigue damage interaction limits. According to A16, the recommended value for the characteristic distance (d) is 50 μm for austenitic stainless steel. However, the development of a visible crack (0.1 - 0.2 mm size) is generally considered as crack initiation. Using the distance of 50 μm for calculating σ_d may be considered as a conservative value for the assessment. Based on detailed investigation with the experimental data, 0.2 mm is considered for defining crack initiation life. The method is illustrated by solving a benchmark problem, as illustrated in Fig. 11.

The experimental benchmark problem is concerned with creep crack propagation in the welded joint incorporated in two standard plane sided 19 mm thick CT specimens which is extracted from ref [Hooton; Bretherton; and Jacques (2003)]. The plane CT specimens are manufactured from a single heat of welded plates made of Type 316 LN steel plates using a matching manual metal arc (MMA) weld combination. The interface between the parent metal and the MMA weld metal is located parallel to the central line of the specimens. The specimens are pre-cracked at room

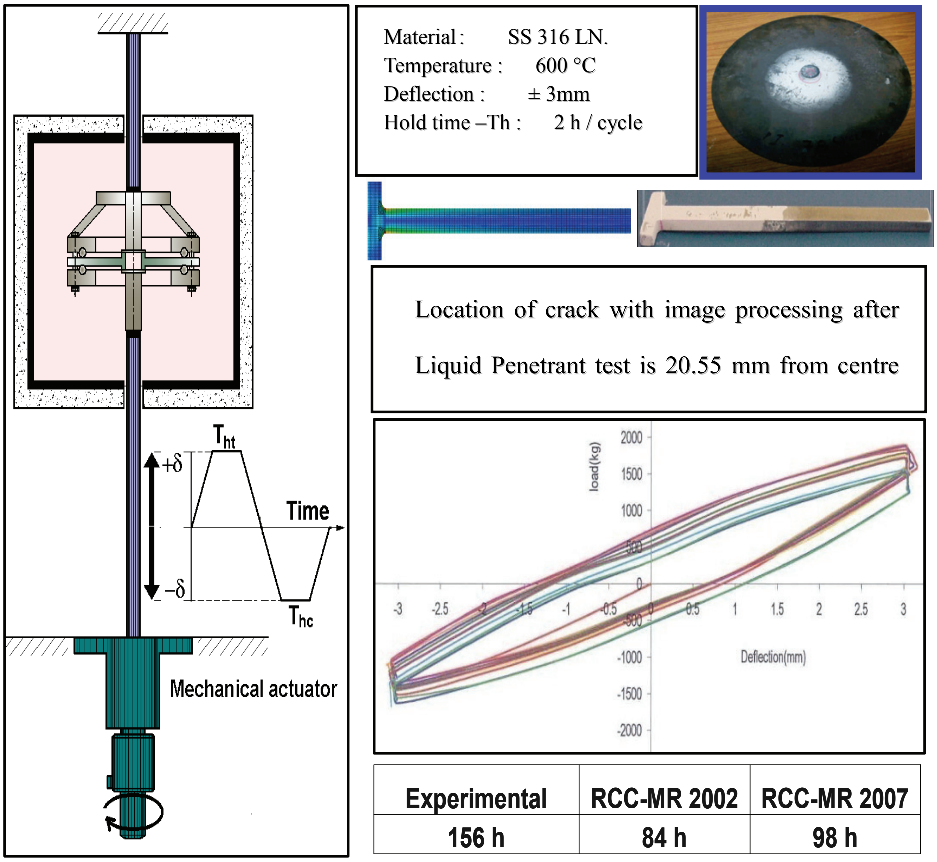

Figure 10: Benchmark test to validate the life prediction methodologies of RCC-MR code

temperature to generate initial crack lengths of 17.58 mm and 17.41 mm. Except for the initial crack size, the geometrical and loading conditions are the same for both specimens, which are shown in Fig. 11. The creep crack propagation tests were conducted in air at 823 K by applying a constant axial load of 20 kN throughout the duration of the test. The times taken for creep crack growth to 0.2 mm were found to be 453 h and 547 h, respectively, which are considered as creep crack initiation times for the two specimens. The same has been predicted with 'σ_d approach'. The comparison indicated that there is scope for improvements in the present approach, particularly in the applications of multi-axial creep rupture criteria, Neuber's rule for estimating elastic plastic strain range and relaxation behavior.

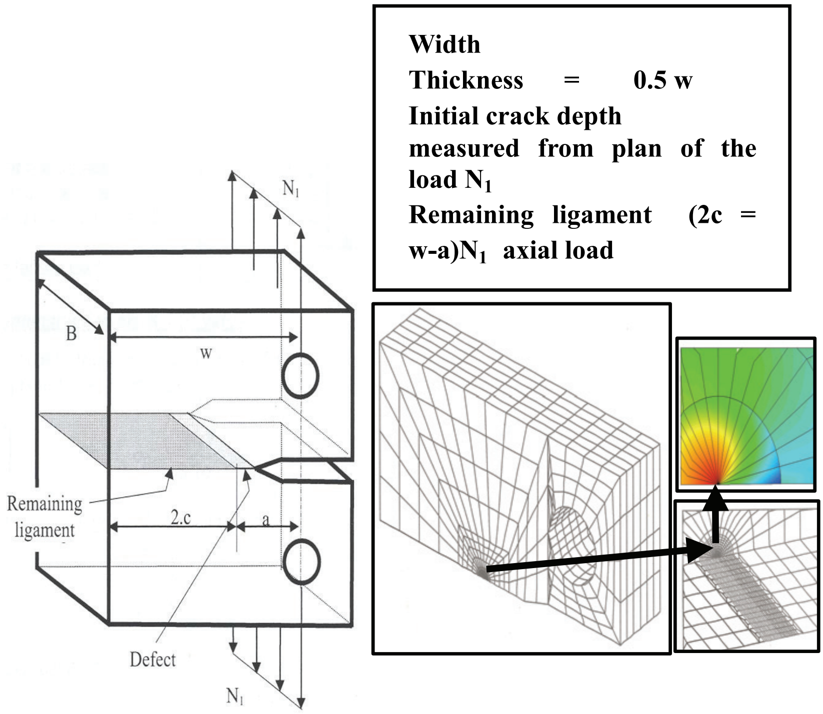

Figure 11: Details of benchmark problem on life prediction of structures with defects

The improved results were compared with detailed elastoplastic analyses (Tab. 2). More details can be seen in ref [Chellapandi, Chetal and Baldev Raj (2005)].

Table 2: Creep life prediction of CT Specimen

Specimen	Initial crack length- a (mm)	Creep crack initiation life - Trd (h)				
		Experiment	A16	Improved	HRR*	FEM
1	17.58	453	4618	435	233	309
2	17.41	547	11360	451	345	345

4.4 Establishing allowable number of repair welds in fuel pin end plug welds

Each fuel subassembly has 217 fuel pins, which contain MOX fuel. The manufacturing of fuel pins is the most challenging activity, in particular, the welding of end plug after inserting the fuel pellets and other structural elements within the clad. Strategy for rejection of pins with repaired welds should be adopted carefully to maximize recovery during manufacture. The fuel pin is made of 20% cold worked D9 material (15 % Cr-15 % Ni –Mo-Ti alloy) and end plug is made of SS 316 LN. The temperature in the region of the end plug is decided by the core outlet temperature (833 K) under steady state operation and the maximum fission gas pressure accumulated at the end of 100 GWd/t burnup is 6 MPa. Under this environment, the thermal creep damage is the main governing failure mode for this weld. Since, there is no established analysis tool available to qualify the repair weld, an experimental route is followed to recommend the acceptable number of weld repairs for the end plug [Rosy Sarkar (2010)].

The life of fuel pin in the reactor is 2 y. Based on appropriate simulation studies including the effects of fuel and fission gas, the minimum rupture life to be ensured and demonstrated by tests in air under similar pressure and temperature conditions is 80 y. However, the tests are accelerated by applying higher pressure and temperature so that the tests can be completed in a reasonable period. Accordingly, the fuel pins with end plug were tested at 973 K to accelerate the damage under an internal pressure of 20 MPa to account for higher burnups as well as uncertainties in the fission gas release. Application of 'Larson-Miller' formula yields that the minimum rupture time to be ensured is 5.6 d. Fuel pin end plug welds for PFBR are carried out at Advance Fuel Fabrication Facility (AFFF) - Tarapur. A few numbers of welds with 0 to 4 repairs were selected from the production samples for the test purpose. A dedicated test setup has been made to test a set of 36 tubes simultaneously. The application of correct pressure is ensured, by measuring the hoop and longitudinal strains in the vicinity of end plug welds for a few typical pins. The leak is monitored continuously by observing the steady state pressure in the pressure chamber. Once creep rupture takes place, the tube develops a small crack after significant bulging in the heat affected zone. Fig. 12 shows the details of fuel pin end plug, 36 pins test assembly and leaked and bulged fuel pins.

The rupture lives measured for the various test cases are depicted in Fig. 13. The minimum rupture time required (5.6 d) are ensured even for the welds with 4 repairs. However, it is recommended to restrict the repair welds to 2 at this stage. Based on the test data and analysis, a design approach is proposed for the inclusion in RCC-MR: 2007 edition. The additional strength reduction factor derived from these limited tests can also be seen in Fig. 13.

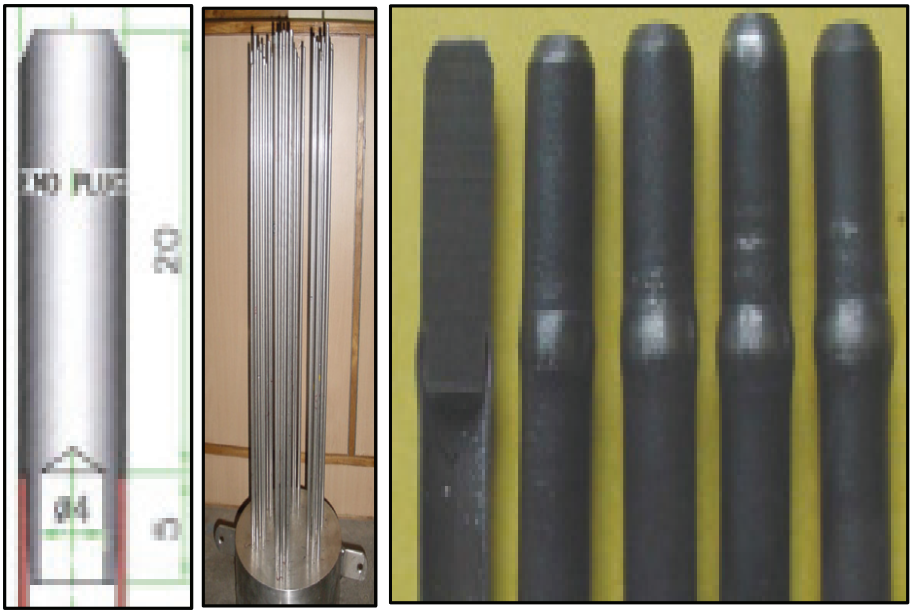

End plug 36 pin Typical leaked pins showing bulging

Figure 12: Fuel end plug, test setup and leaked and bulged pin configurations

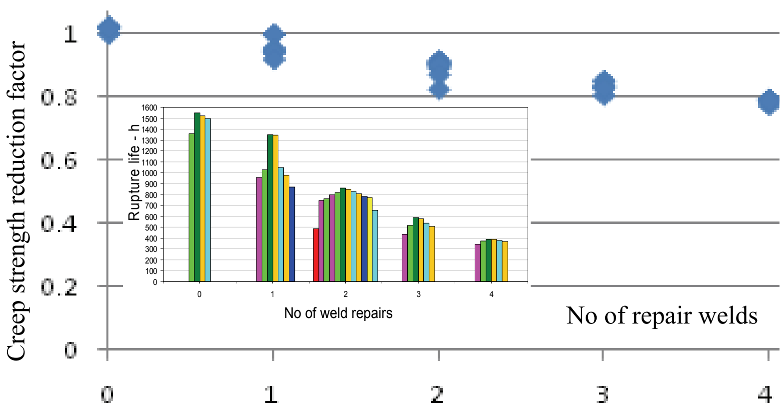

Figure 13: Rupture lives of 36 fuel pins and proposed design rules for repaired welds

4.5 Investigation of various kinds of instabilities

In view of high flexibility associated with large fluid mass, the stability of structures immersed in sodium is investigated by understanding various instability mechanisms. A few of them are highlighted here.

4.5.1 Jet instability

Sodium jets of different temperatures emerging from core subassemblies undergo instability, causing random temperature fluctuations on the adjoining structural wall. This phenomenon is called thermal striping. In particular, the structural wall facing the jet impacts from fuel and its adjacent control subassembly is subjected to high temperature fluctuations (Fig. 14 a) and can cause high cycle fatigue damage. Such failures were reported for French reactor Phenix in the expansion tank as depicted in Fig. 14b [Bettes, Judd and Lewis (1994)]. Thermal striping limits were established based on 'σ-d approach' [Chellapandi, Chetal and Baldev Raj (2009)]. Considering random thermal fluctuations and frequency-dependent thermal attenuation on structural wall, limits are derived at various potential locations in SFR (Fig. 14c). These structures are also subjected to creep-fatigue damage due to major cycles caused by startup, shutdown, grid failures, pump trips, etc. By performing advanced thermal hydraulics analysis using 'Direct Numerical Simulation' technique, the possible temperature fluctuations at various locations in the hot and cold pool components were estimated (Fig. 14d) and found to have comfortable margins w.r.t. proposed limits. More details can be seen in ref [Velusamy, Sundararajan, Chellapandi, Selvaraj and Chetal (200)].

The frequency contents of temperature fluctuations, essential for establishing design rules were obtained from simulated water tests as indicated in Fig. 15. The temperature fluctuations clearly indicate randomness in frequency contents and amplitudes of fluctuations for various simulated conditions.

4.5.2 Fluid elastic instability

The main vessel is the most critical component in the SFR design, since it houses the entire radioactive primary circuit including sodium. Hence, it is designed and constructed respecting strictly the nuclear class 1 rules (RCC-MR for e.g.). Apart from this, certain features are introduced to enhance its structural reliability, viz., (i) choice of highly ductile construction material, austenitic stainless steel type SS 316 LN, (ii) maintaining relatively low operating temperatures so that there are no significant creep and hot cracking issues and (iii) periodic inspection during its service. In order to cool the vessel, a novel cooling system is incorporated in the main vessel, which consists of weir shell and additional baffle (Fig. 16).

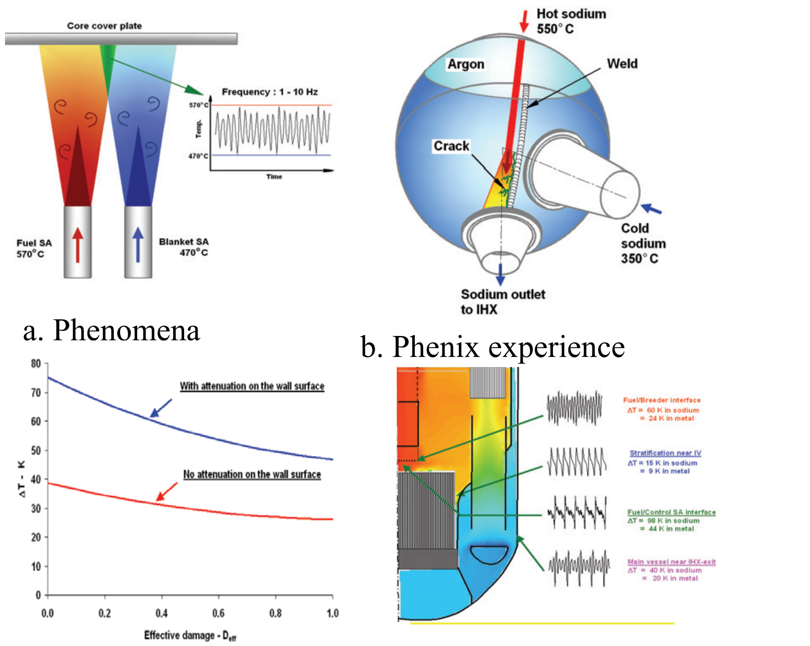

a. Phenomena b. Phenix experience

c. Proposed limits d. Numerical simulation for PFBR

Figure 14: Thermal striping: Phenomenon and Analysis

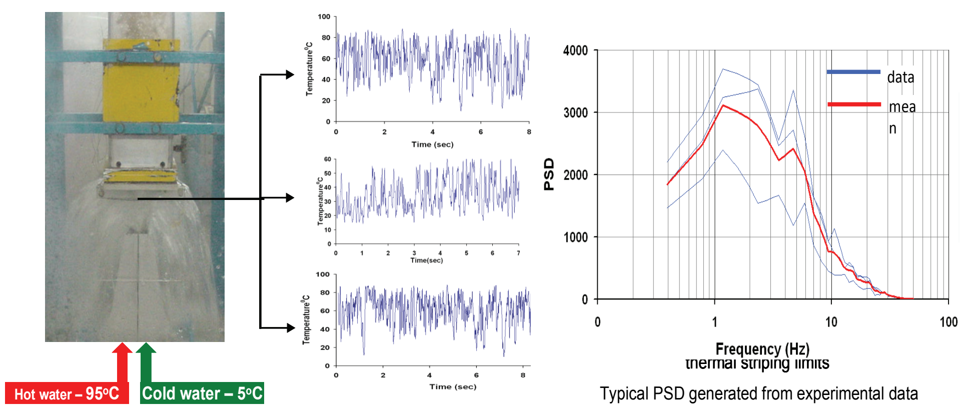

Figure 15: Simulation of thermal striping in a water models

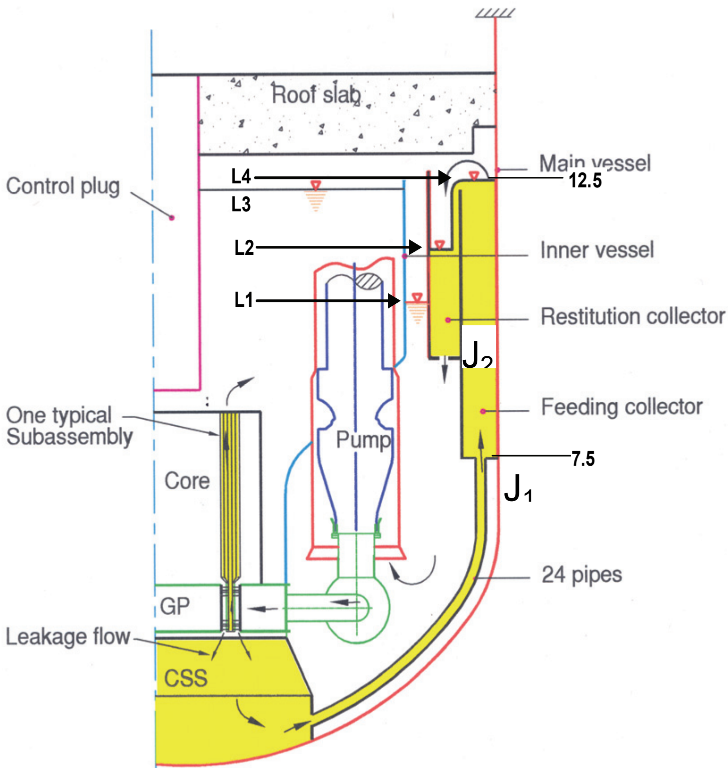

Figure 16: Main vessel cooling system

When the cold sodium flows over the weir shell and falls back on the free level of restitution collector, dynamic fluid forces are developed on the free surfaces of feeding and restitution collectors due to sloshing of liquid surfaces under small perturbation of weir shell. These forces enhance the shell displacements, resulting in unstable vibration, termed as fluid elastic instability. This phenomenon is illustrated in Fig. 17.

With the fundamental understanding, self induced fluid forces on the weir shell due to sloshing of liquid free levels are identified and analytical expressions are derived. Using the modal super position principles, the modal based non-linear dynamic equilibrium equations are written. Subsequently, the equations are solved by direct integration technique using Newmark-β method employing the natural frequencies and mode shapes computed numerically through CAST3M code. Evolution of weir displacements and wave heights are obtained for the experimental

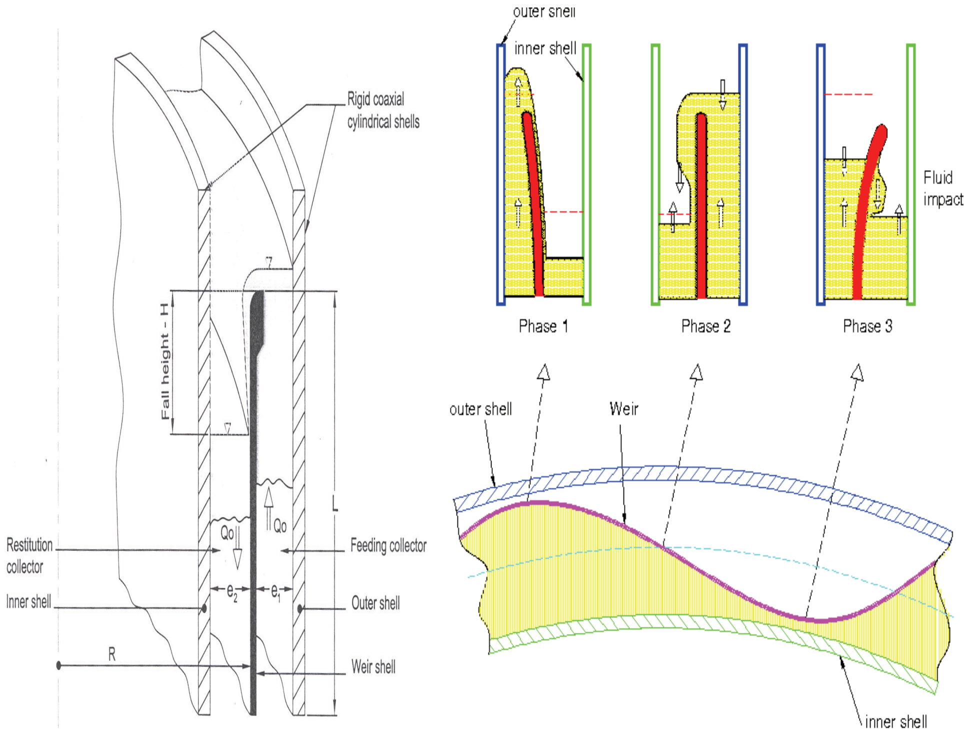

Figure 17: Schematic sketch of idealised cooling system and weir instability mechanism

benchmark problem in which 1/5 scale model of DFBR, the Japanese fast breeder reactor is simulated. The fall time and dynamic responses are predicted satisfactorily even with a few available input data. Subsequently, PFBR weir shell was analysed and noted that the flow rate and associated fall height during fuel handling condition are critical. Further, the analysis also indicated that the weir shell vibrations are negligible for the damping value >1 % and for the damping of 0.5 %, the maximum amplitude is $\sim$ 3.5 mm (Fig. 18). More details can be seen in [Chellapandi, Chetal and Baldev Raj (2008)].

From the literature it is confirmed that the minimum damping of weir is >1 %. Hence, weir shell would be stable during fuel handling operations and thereby satisfying all the operating conditions. The computer code developed for this analysis has also been used for understanding the phenomena and similarity principles, apart from utilizing it for analysis of weir shell response of thermal baffles of PFBR. Hydraulic tests on the full scale sector water mockup were conducted to identify

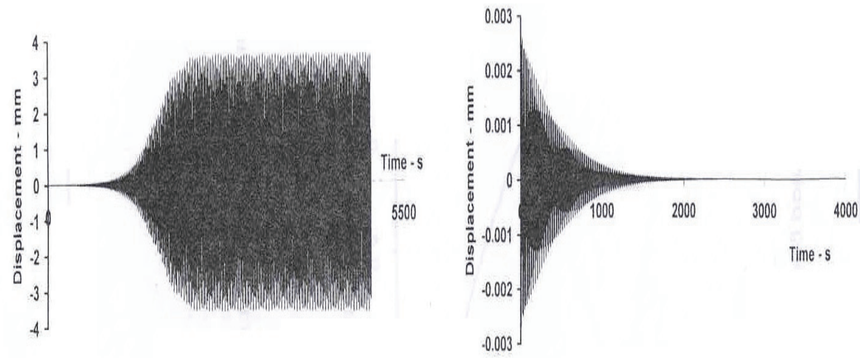

Figure 18: Displacement of PFBR weir shell during fuel handling condition

the instability zones and compared with the theoretical predictions. The study has shown excellent comparison on dynamic displacement of weir shell crest as well as the instability regimes (Fig. 19).

4.5.3 Elastic instability of thin shells under seismic induced forces

Elastic instability causes buckling. In the reactor assembly of SFR, the main vessel, the inner vessel and the thermal baffles are thin walled shell structures, prone to buckle. The buckling of thin shells under randomly varying seismic induced forces calls for sophisticated analysis techniques such as time domain analysis. The conventional seismic responses analysis provides time dependent stress and pressure distributions, which is performed in the first phase.

Subsequently, elastic instability is investigated by 'Bifurcation analysis'. Fig. 20 shows a 3-D finite element mesh generated for the seismic analysis, which includes thin vessels, fluid and fluid free surfaces. The dynamic pressures developed on the main vessel, inner vessel, inner and outer thermal baffles which are derived from the analysis at a critical instant are depicted in Fig. 21.

Due to the kind of pressure fields generated on the surfaces shown in Fig. 21, the upper cylindrical portion of main vessel is subjected to shear buckling (Fig. 22a). The inner vessel under the combined action of static pressure of 4 m of sodium head and dynamic pressure developed under vertical seismic excitations buckles at the toroidal portion (Fig. 22b). The inner and outer thermal baffles adjacent to main vessel which are subjected to dynamic pressure distribution developed under horizontal and vertical excitations, undergo asymmetrical buckling as shown in Fig. 22c and Fig. 22d. More details can be seen in ref [Chellapandi, Chetal and Baldev

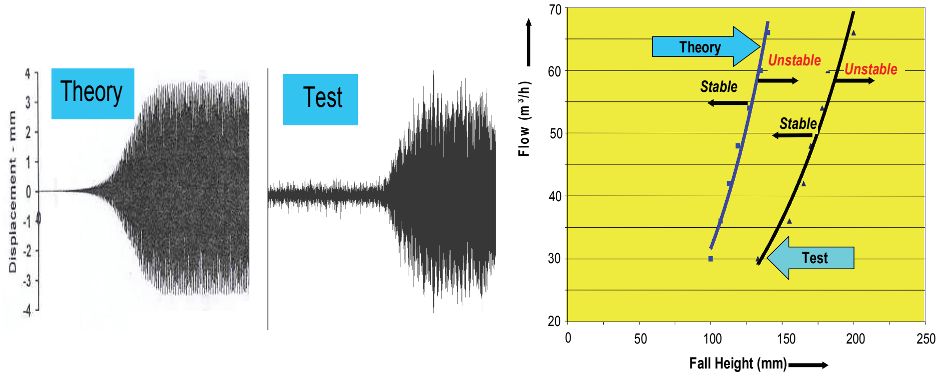

Dynamic displacement of crest of thermal baffle

Weir instability regimes

Figure 19: Theoretical and experimental simulation of weir instability

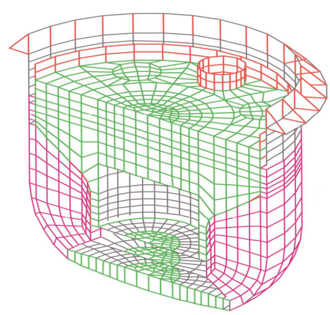

Figure 20: Finite element mesh of reactor assembly

Raj (2008)].

The elastic instability has been simulated on 1/13th scaled down models of the main vessel cylindrical portion and inner vessel by imposing the respective peak forces. The prediction of shear buckling mode and critical buckling load for main vessel straight portion is shown in Fig. 23. More details can be seen in ref [Athiannan (1998)]. Elastic instability of torus shell portion of the inner vessel subjected to pressure and axial forces acting along the stand pipes, is simulated experimentally and numerically. A typical comparison is shown in Fig. 24. More details can be seen in ref [Bose, Thomas, Palaninathan, Damodaran and Chellapandi (2001)]. The critical buckling load mode shapes are predicted by using CAST3M computer code. It is found that the CAST3M code used for the shear buckling analysis of

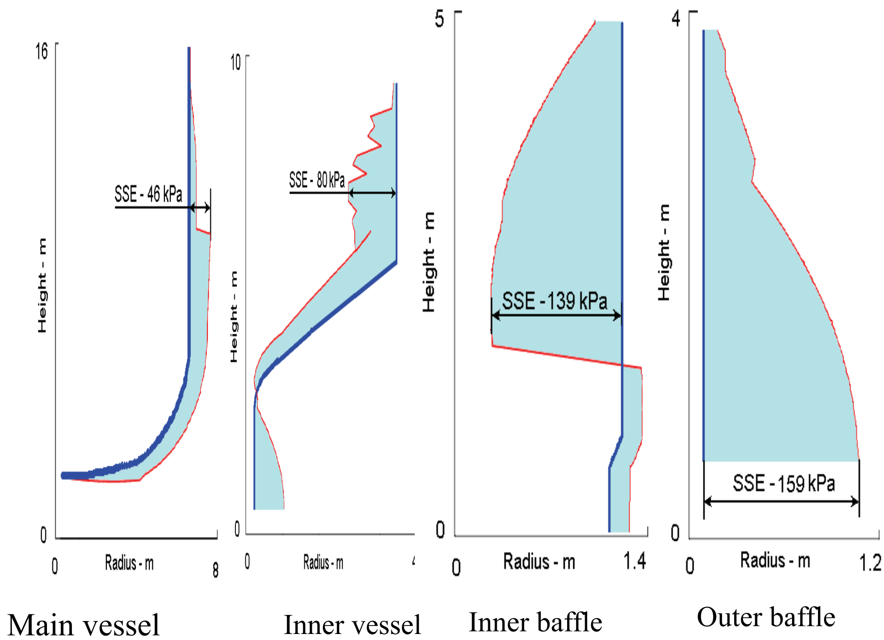

Figure 21: Peak dynamic pressuredistribution at a critical time step w.r.t buckling

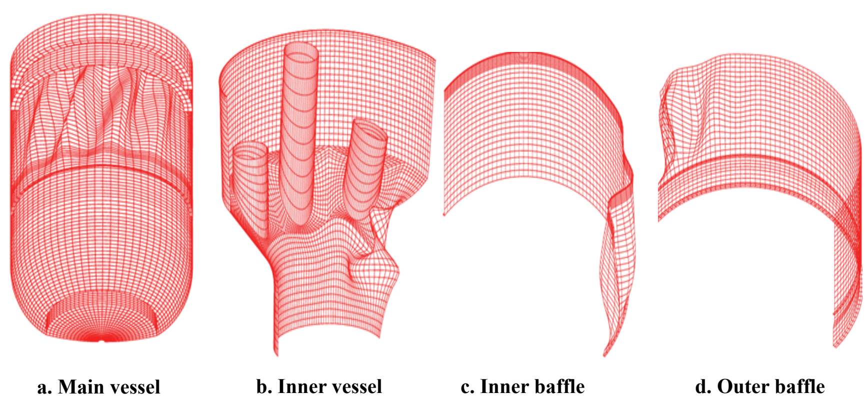

Figure 22: Buckling mode shapes of thin vessels of reactor assembly

Test mode shape

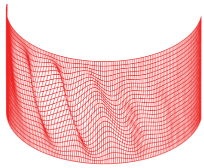

Predicted mode

Thickness mm	Imperfection x thickness	No.of tests	Buckling load-t Test	Buckling load-t FEM
0.8	2.2-3.8	4	33-54	28-32
1.0	1.1-4.2	4	50-69	42-56
1.25	1.2-3.4	4	60-73	72-99

Comparison of critical buckling load

Figure 23: Experimental and numerical simulation of shear buckling instability for thin shells

thin shells over-predicts the critical shear buckling load by 20 % for some cases indicated in Fig. 23 [Athiannan (1998)].

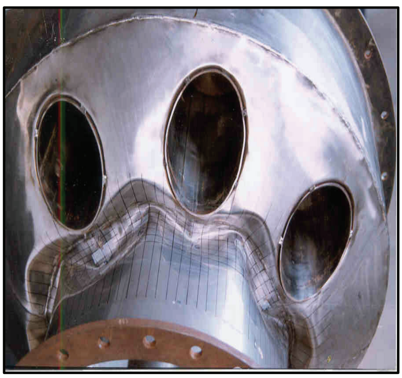

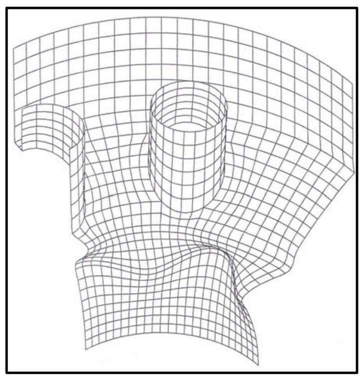

Loading - P	Geometrical imperfection - mm				P_{exp}	P_{FEM}	$\frac{P_{exp}}{P_{FEM}}$
	Lower shell	Torus	Cone	Upper shell			
Pressure – MPa	-1.2 to 1.4	-1.4 to 1.4	-2.7 to 1.5	-1.3 to 1.7	0.9	0.95	0.95
Axial force - t	-2.5 to 1.3	-1.2 to1.1	-2.9 to 1.7	-1.8 to 2.5	1.61	1.40	1.15
Pressure + Axial force	-1.2 to 1.1	-1.7 to 1.4	-1.1 to 1.3	-1.8 to 0.9	0.175 1.180	0.151 1.180	1.16

Figure 24: Simulation of buckling mode under pressure and axial force for inner vessel

4.5.4 *Parametric instability of thin shells under seismic induced forces*

Flexible components and structures, such as core subassemblies and thin wall shell structure in reactor assembly can develop unbounded out-of-plane displacements (bending), under cyclic in-plane force, lower than the critical buckling force corresponding to peak value. This phenomenon is called parametric instability, which is basically due to coupling of vibration and buckling mode shapes. One of the sources of cyclic membrane forces are high initial forces caused by a design basis seismic earthquake. This phenomenon is to be analyzed critically for thin thermal baffle, which are subjected to random pressure in the sodium volume confined in the feeding and restitution collectors (Fig. 16). Similarly, the sloshing displacements of sodium free surfaces and displacements of core subassemblies in the horizontal directions can also enter in to the zone of unbounded displacements under vertical seismic excitations. The parametric instabilities in thermal baffle, core subassemblies and liquid free levels (Fig. 25) have been calculated based on analytical, numerical and experimental studies.

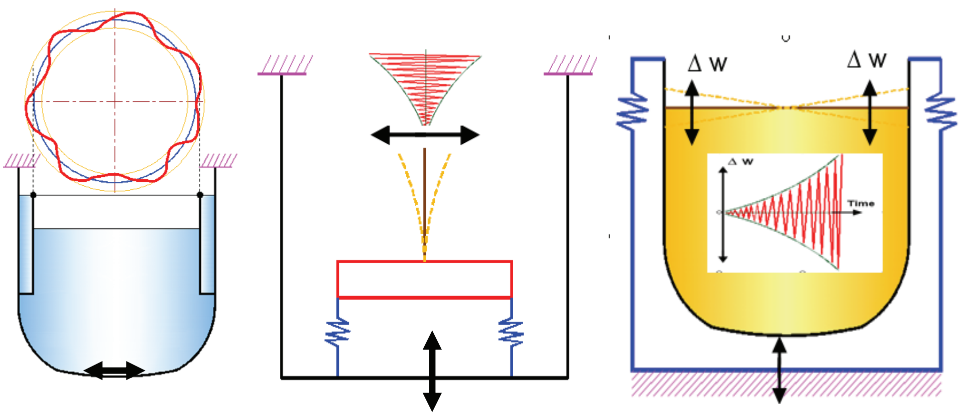

Figure 25: Parametric instabilities in reactor assembly system

The dynamic equilibrium equations consisting of inertial force, damping force and internal forces are derived applying finite element principles and finally expressed in following matrix form:

$$[M]\{\ddot{X}\}+[C]\{\dot{X}\}+[K_L]\{X\}+[K_{NL}]\{X\}=0 \quad (1)$$

where [M], [C], [K_L] and [K_{NL}] are mass (representing inertial force), damping (representing dissipative force), linear and non-linear stiffness matrices (representing internal force). {X} is the displacement vector. The instability of above equation is investigated by transforming the equation-1 using natural vibration modes shapes, as per modal superposition technique. The resulting equations are:

$$\eta_n + 2\xi\,\omega_{m\eta n} + \omega_n^{2\eta}{}_n + \sum[\sum d_{nms}\cos\omega_s t + \sum e_{nms}\sin\omega_s t]\eta_n = 0 \qquad (2)$$

where η_n is the projected displacements, ω_n is natural frequency, ξ is the modal damping factor, ω_s is excitation frequency, d_{nms} and e_{nms} are the components of projected non-linear stiffness matrix, which are coupled. In this formulation, the pressures on the wall surfaces are expressed in frequency domain (s represents frequency component).

The stability analysis of equation-2 is investigated using 'Hsu's Criteria' [Hsu (1963)], by gradually increasing the pressures proportionally, that is, indirectly applying the higher peak ground acceleration at the reactor assembly foundation. The resulting stability chart is depicted in Fig. 26, which indicates that the thermal baffle is free from risk of parametric instability, if peak ground acceleration (PGA) does not exceed 0.3 g. PGA value for the PFBR site, i.e. Kalpakkam, is 0.156 g. Hence, there is no concern of such instability. The parametric instability of thin cylindrical shell representative of thermal baffle has been simulated numerically as well as experimentally (Fig. 27).

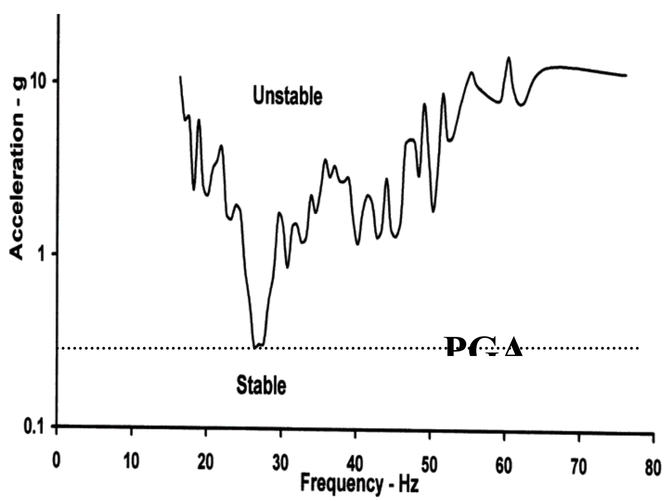

Figure 26: Parametric instability chart for thermal baffle

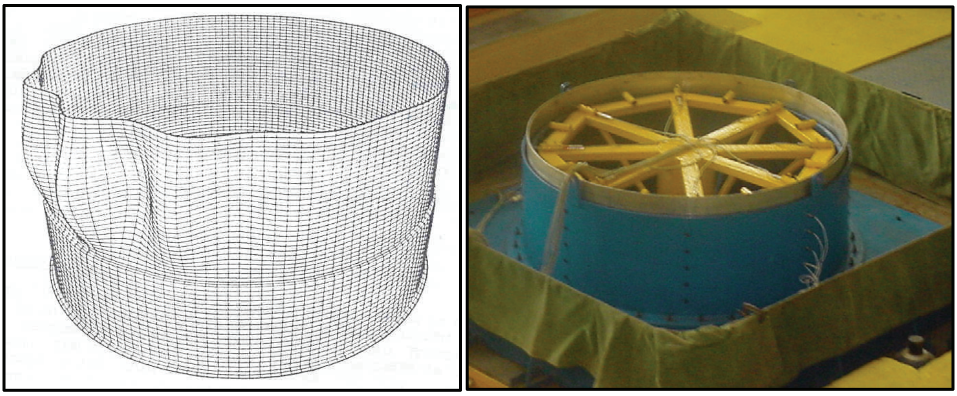

Figure 27: Numerical & experimental simulation of parametric instability of thermal baffle

4.5.5 Whirling instability of sodium pumps with hydrostatic bearing

In pool type SFR, the primary pump delivering sodium flow to the core, generally has a long shaft ($\sim$12 m). The pump is supported by thrust bearing at the top, which faces the normal atmosphere and the bottom portion (impeller side) is immersed in sodium pool. In order to have good vibration stability, hydrostatic bearing (HSB) operating in sodium, is used, since mechanical bearing with oil lubricant is not permissible in sodium due to safety reason. Since, the pump has to operate at variable speeds in the range of 200-590 rpm, it is important to ensure that there is no instability at any operating speed. Fig. 28 shows the schematic of PFBR pump.

When the natural frequency matches with any speed of pump, whirling instability may occur. The pump natural frequency is $\sim$10 Hz corresponding to the nominal speed of 590 rpm and predominant frequency of seismic excitations also lies in the range of this frequency. So, dynamic stability of pump should be investigated critically. Towards this, fluid mechanics analysis of HSB is carried out in the first phase to determine the stiffness and damping characteristics of bearing including gyroscopic effect, as it rotates. The resonant speed obtained through dynamic response analysis is 700 rpm which has a margin of 1.2 against the nominal speed (Fig. 29).

The maximum amplitude of shaft is limited to 160μ, when the shaft runs even at resonance speed. At 15% speed, the vibration levels are insignificant. Theoretical model has been developed for predicting the dynamic behavior and stability of the

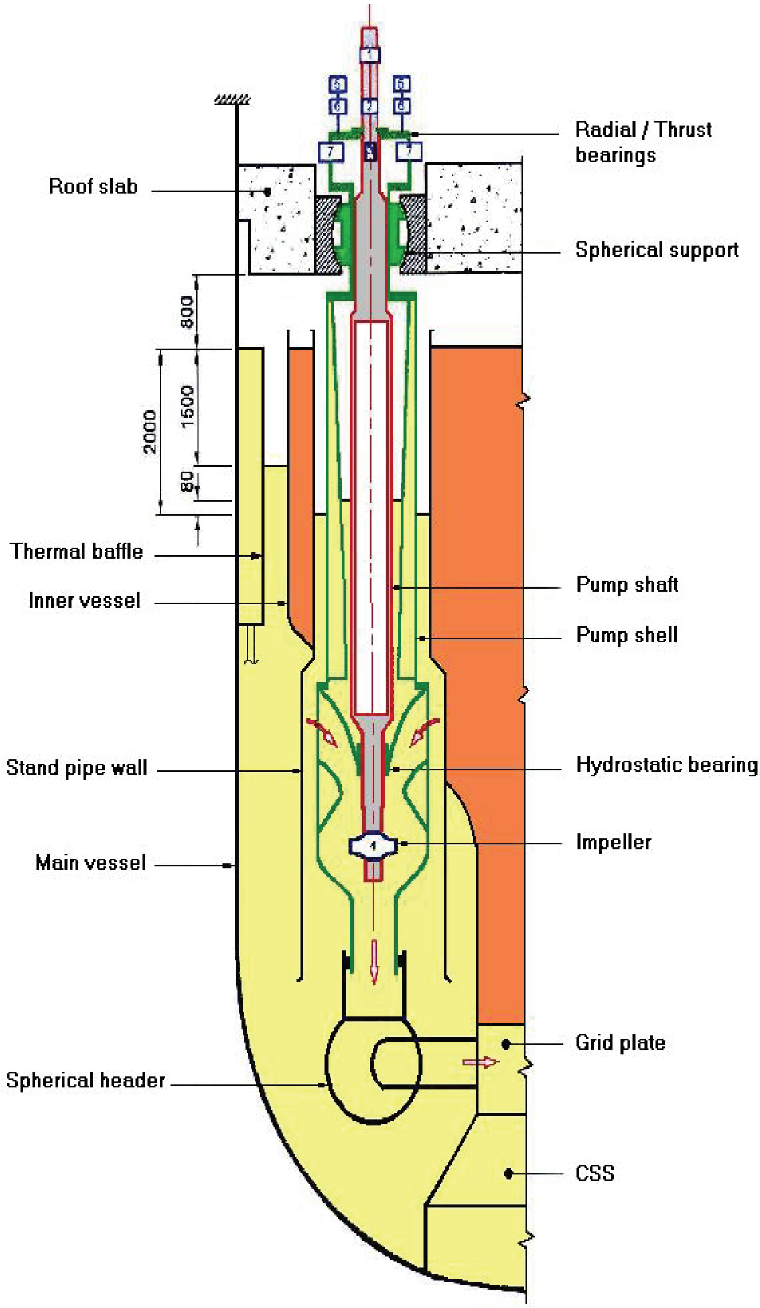

Figure 28: Schematic of primary pump

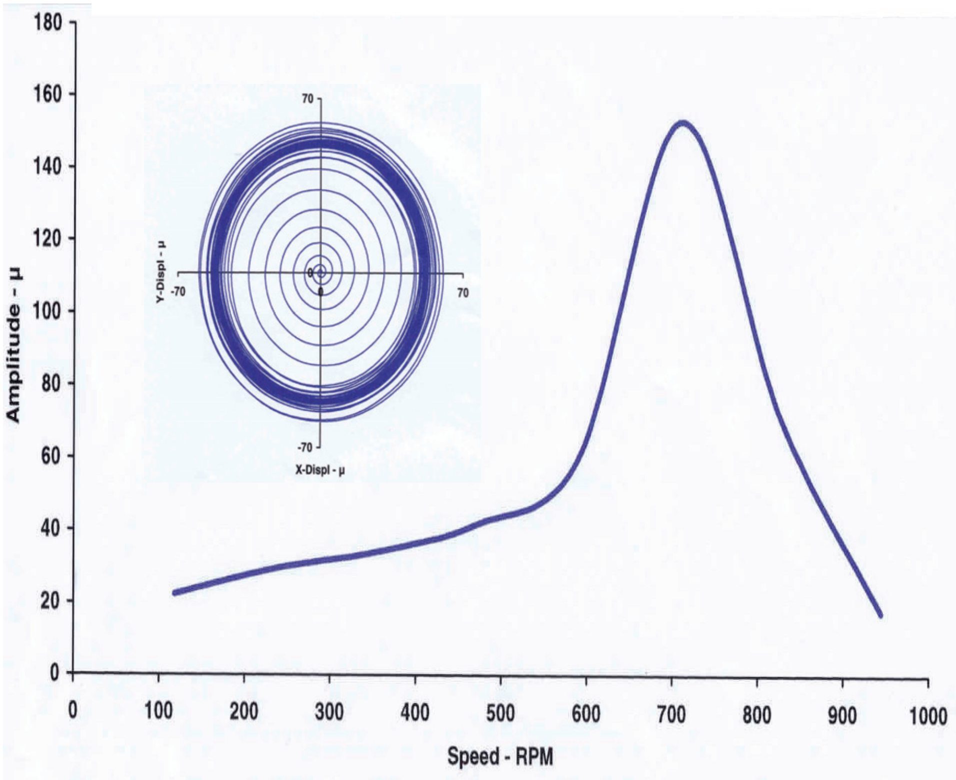

Figure 29: Pump shaft resonance

pump shaft with HSB. Forward and backward whirling instability has been investigated and found that the pump can enter into unstable regime once speed is greater than 1.5 times rated rpm (Fig. 30). In order to raise the conference, benchmark experiments have been conducted to simulate both resonance and instability (Fig. 31).

4.6 High strain rate deformation due to fast transient fluid-structure interaction

As a part of safety study, the main vessel has to be analysed for the structural integrity under postulated core disruptive accident (CDA) loadings. The accident scenario depicts complicated deformation patterns due to impact of shock / pressure waves, as indicated in Fig. 32. Deformation of bottom torispherical portion in the early stage and bulging of upper cylindrical portion can be observed. The deformations occur rapidly within 1 s.

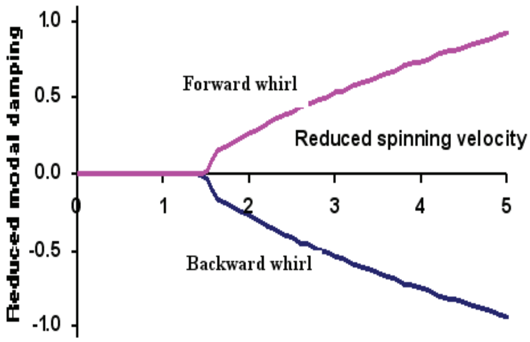

Figure 30: Pump shaft instability

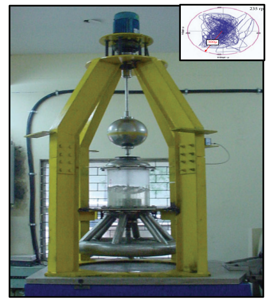

Figure 31: Experimental test setup

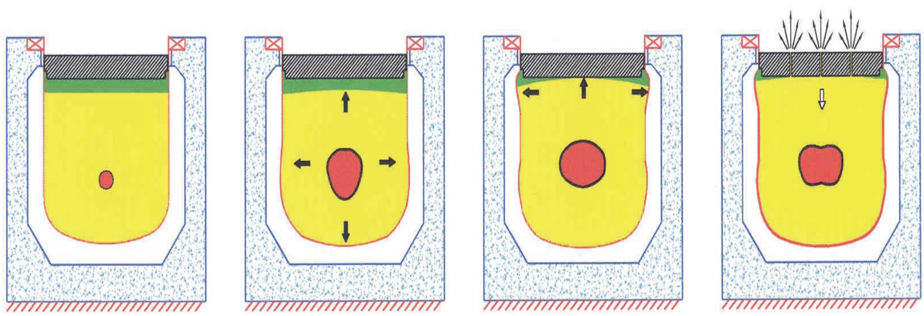

Figure 32: High plastic strain rate deformation sequence of main vessel under CDA

In order to predict such rapid deformations numerically, a computer code has been developed, which simulates large displacements, high strain rate plastic deformations, complicated gas bubble motions, large deformations of liquid, fluid structure interactions and pressure wave propagation, sodium slug impact and consequent local pressure rise in the sodium at the bottom of the top shield. The computer code employs Arbitrary Lagrangean Eulerian (ALE) formulation for fluids and convected co-ordinate formulation for structures.

Specific tests were conducted by using appropriate low density explosive to simulate the deformation patterns representing the CDA scenario. The prediction of deformation for a typical vessel ($1/30^{th}$ scaled down models of main vessel) is shown in Fig. 33 and can be found to be extremely satisfactory. With extensive

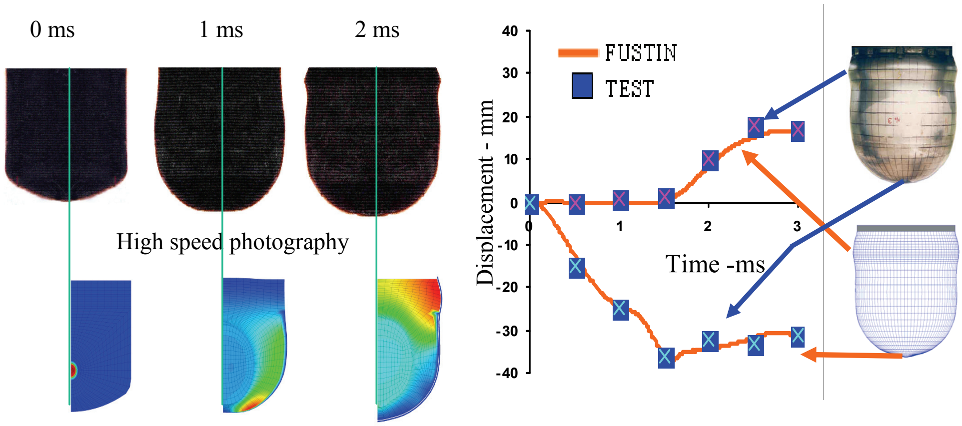

Figure 33: Deformation for 1/30th scaled down models of main vessel under simulated CDA

numerical and experimental investigations, the structural integrity of main vessel is ensured with high level of confidence under CDA. Fig. 34 shows the numerically predicted core bubble expansion at a few discrete intervals during core disruptive accident. The details are given in ref [Chellapandi, Chetal and Baldev Raj (2010); Chellapandi, Chetal and Baldev Raj (2010)].

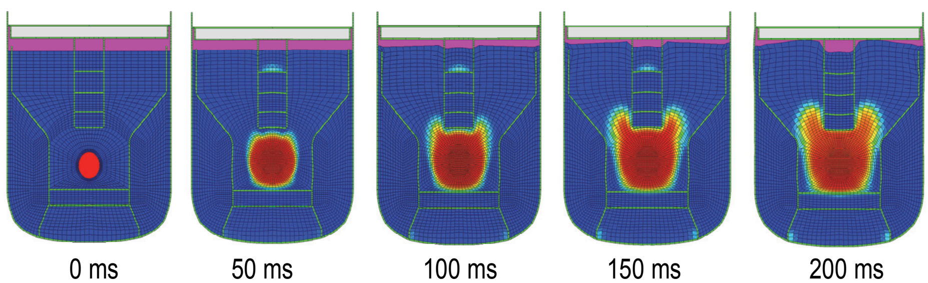

Figure 34: Deformation behaviour of reactor assembly components under CDA

5 Future direction: development of new design rules

The experience and expertise accumulated over the years by solving structural mechanics problems specific to PFBR, are instrumental to develop the following new design rules in the structural design of SFR components. These rules are recommended for the consideration of future version of RCC-MR, the French design rules for mechanical design of SFR components.

5.1 Interaction among plastic collapse, buckling and tearing instability

In the failure assessment diagram of CEGB-R6 [Milne, Anisworth, Dowling and Stewart (1988)], the global instability of components is governed by the interaction between plastic collapse and tearing instability. It is experimentally observed that, in case of SFR components, which are basically thin walled shell structures, there is strong interaction of buckling. This is illustrated in Fig. 35. Such interaction diagram is being developed.

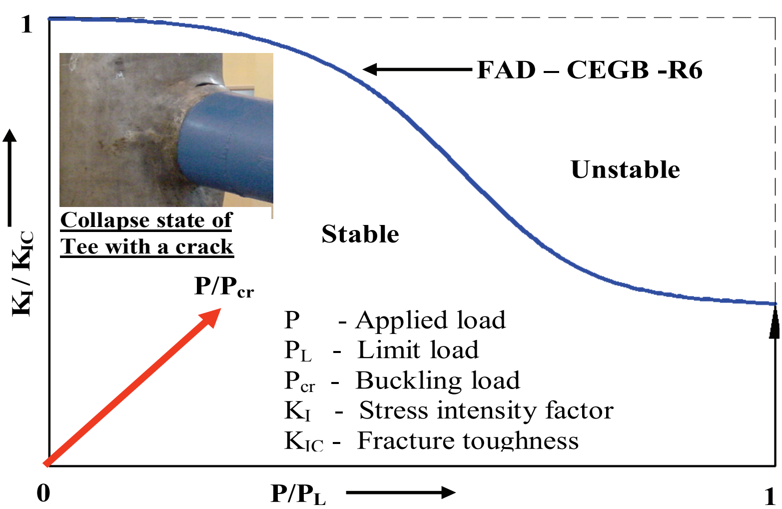

Figure 35: Effect of buckling on the failure assessment diagram: New proposal

5.2 Effect of loading rate on buckling of thin shells

It is seen that the critical buckling loads under dynamic forces acting on the thin shells would be lower with interaction between vibration and buckling modes, due to parametric instability. However, under high loading rate, the buckling can be stable and associated critical buckling load is much higher than the critical buckling load corresponding to peak force [Combescure (1988)]. With this experience, design rules are proposed, which provides a relation between the (critical buckling load under dynamic load/static buckling load corresponding to peak force) 'Vs' frequency of loading. Fig. 36 shows a possible trend on the effect of frequency.

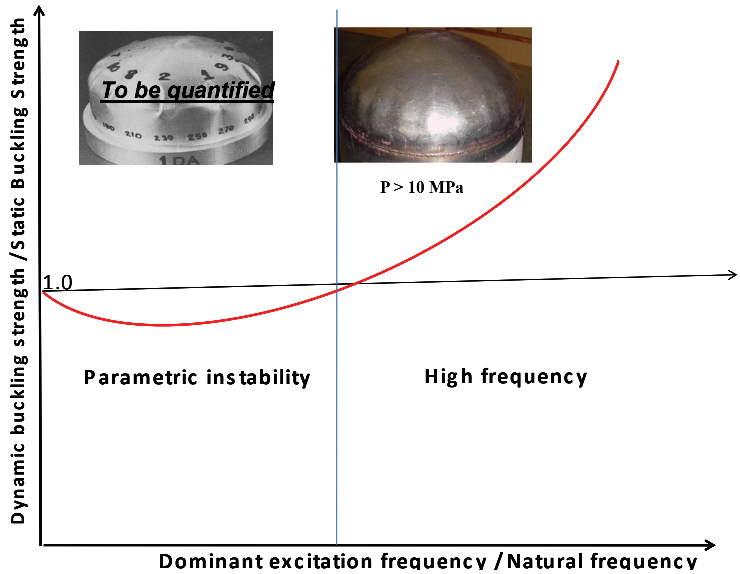

Figure 36: Effect of loading frequency on the buckling strength

5.3 Buckling of dished head under combined pressure and concentrated force

Design rules exist for the dished heads under internal pressure. The effect of axial force acting at the interface between torus and spherical portions is investigated in ref [Murakami, Yoshizawa and Hirayama (1997)]. New design rules are to be generated in the form shown in Fig. 37.

5.4 Effect of cyclic thermal loads on buckling strength

The cyclic thermal loads with or without mechanical forces may cause ratcheting deformations. Such phenomenon cause local deformations in the zone of cyclic temperature variations. These deformations could affect the buckling load [Combescure and Brochard (1991)]. To quantify the effects, design rules should be proposed in the form of curve shown in Fig. 38.

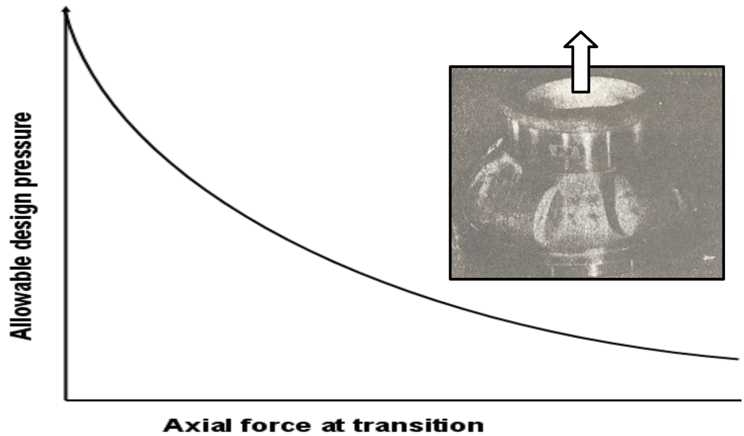

Figure 37: Effect of axial force on buckling of torispherical head under internal pressure

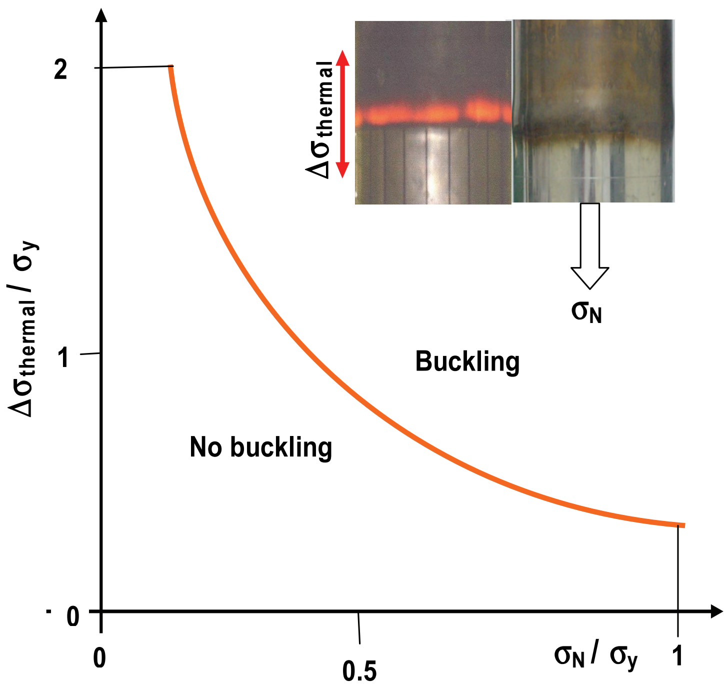

Figure 38: Effect of axial stress on themal ratcheting

6 Concluding remarks

Mechanical design of SFR components is carried out by detailed analysis involving numerical and experimental simulations of advanced concepts in mechanics. This approach has been instrumental in achieving optimum wall thicknesses for the thin shells of reactor assembly components, with the enhanced safety. The application of advanced concepts, apart from helping to finalise the design of PFBR, forms strong basis for developing new design rules for the consideration of inclusion in the future applicable design codes, such as RCC-MR. Further, they provide important input for assessing the acceptability of some deviations observed during manufacturing of SFR components, to save cost and time. Thus, the application helps indirectly to reduce the construction time resulting in improved economy. During this course, a need is felt for the application of new concepts in applied mechanics viz. interaction among plastic collapse, buckling and tearing instability, effect of loading rate on buckling of thin shells, buckling of dished head under combined pressure and concentrated force and effect of cyclic thermal loads on buckling strength, towards design of future sodium cooled fast reactors.

References

Athiannan, K. (1998): Investigation of buckling of thin shells, *Phd Thesis, Dept. of Applied Mechanics, IIT, Madras.*

Baldev Raj (2008): Science and technology of fast breeder reactor programme in India: Challenges and Achievements, *Prof. Jai Krishna Memorial award Lecture, INAE Annual convection, Goa*, Dec 5-6,

Bettes, C; Judd, A. M.; Lewis, W. W. J. (Nov 1944): Avoiding thermal striping damage: experimentally based design procedures for high cycle thermal fatigue, *IWGFR/90, Specialists Meeting on Correlation Between Material Properties and Thermohydraulics Conditions in LMFBRs, Aix-en-Provence, France*, 22-24.

Bose, M. R. S. C.; Thomas, G.; Palaninathan, R.; Damodaran, S. P.; Chellapandi, P. (2001): Buckling investigations on a nuclear reactor inner vessel model, Experimental Mechanics, *SAGE Publications*, Vol. 41, No. 2, pp. 144-150.

Chellapandi, P.; Chetal, S. C.; Baldev Raj. (2009): Investigation of structural mechanics failure modes in FBR, pressure vessels and piping: codes, standards, design and analysis, Narosa Publishing House, New Delhi.

CEA (2003): `http://www-cast3m.cea.fr/cast3m/`. *CAST3M – User Manual.*

Chellapandi, P.; Alwar, R. S. (Aug 1993): Improvements in chaboche viscoplastic model with reference to LMFBR applications, *Proc. Seminar on Inelastic Analysis, Fatigue, Fracture and Life Prediction, Session-5, Paris*, 23-24, pp. 1-8.

Chellapandi, P.; Chetal, S. C.; Bhoje, S. B. (June 2000): Theoretical and experimental investigations on thermal ratchetting of main vessel of an FBR, Tran. Indian Institute of Metals, Vol.53, No.3, pp. 391-399.

Chellapandi, P.; Bhoje, S. B.; Alwar, R. S. (April 1996): Life prediction of control plug of a pool type fast breeder reactor based on viscoplastic deformations, *6th Int. Conf Creep and Fatigue I Mech E, London*, 16-18, pp. 411-423.

Chellapandi, P.; Chetal, S. C.; Baldev Raj. (June 2005), Assessment of σ-d approach for creep damage estimation of FBR components with crack like defects at welds, *Int. Journal of Pressure Vessels and Piping*, Vol. 82, pp.739-745.

Chellapandi, P.; Chetal, S. C.; Baldev Raj. (Aug 2009): Thermal striping limits for components of sodium cooled fast spectrum reactors, *International Journal of Nuclear Engineering and Design*, Vol. 239, pp. 2754-2765.

Chellapandi, P.; Chetal, S. C.; Baldev Raj. (June 2008) :Investigation of fluid-elastic instability of weir shell in a pool type fast breeder reactor, *Advances in Vibration Engineering, The Scientific Journal of the Vibration Institute of India*, Vol. 7, No. 2, pp. 111-126.

Chellapandi, P.; Chetal, S. C.; Baldev Raj. (Aug 2008): Investigation on buckling of FBR vessels under seismic loading with fluid structure interactions, *Journal of Nuclear Engineering and Design*, Vol. 238, pp. 3208-3217.

Chellapandi, P.; Chetal, S. C.; Baldev Raj. (Oct 2010): Structural integrity assessment of reactor assembly components of a pool type sodium fast reactor under core disruptive accident - part 1: Development of computer code and validations, *Journal of Nuclear Technology*.

Combescure, C.; Brochard, J. (Aug 1991): Recent advances on thermal buckling new results obtained at CEA, *Tran. 11th Int. Conf on Structural Mechanics in Reactor Technology (SMiRT11), Tokyo, Japan,* vol. E, 1823, pp. 299-307.

Combescure, A. (1988): Upon the design of structures in case of seismic buckling, *Proc. Of 6th Int. Conf Pressure Vessel Technology*, Vol. 3, pp. 1753-1758.

Hooton, D. G.; Bretherton, I.; Jacques, S. (Nov 2003): Application of the sigma-(d) method for the estimation of creep crack incubation at austenitic weld boundaries, *Proc 2nd Int. Conf. on Integrity of High Temperature Welds, London*, 10-12, pp. 425-434.

Hsu, C. S. (Sep 1963): On the parametric excitation of a dynamic system having multiple degrees of freedom, *Journal of Applied Mechanics*, pp. 367-372.

Milne, I.; Anisworth, R. A.; Dowling, A. R.; Stewart, A. T. (Feb 1988): Assessment of the integrity of structures containing defects, *R/H/R6- Rev. 3.*

Murakami, T.; Yoshizawa, H.; Hirayama, H. (1997): Buckling strength of elliptical heads with core support structure under vertical and horizontal loads, Seismic Resistance of Fast Breeder Reactor Components Influenced by Buckling, Kajima Institute Publishing Co., Ltd. Japan, pp. 388-393.

Rosy Sarkar. (2010): A design approach for establishing creep strength reduction factor for repair welds, *M.E Thesis Report.*

RCC-MR (2000): Design and Construction rules for mechanical Components for FBR Nuclear IslandsI, Section I, Subsection B, Class 1 Components, *AFCEN*.

RCC-MR (2002): Appendix A16: Guide for leak before break analysis and defect assessment, *AFCEN*.

Suresh Kumar, R.; Chellapandi, P.; Chetal, S. C. (Oct 2003): Fatigue damage analysis on ring stiffener of PFBR inner vessel, 4^{th} *Conf. on Creep-fatigue and Creep-fatigue Interaction, IGCAR, India*, 8-10.

Velusamy, K.; Sundararajan, T.; Chellapandi, P.; Selvaraj, P.; Chteal, S. C. (May 2005): Investigations of thermal striping in primary circuit of prototype fast breeder reactor, *Proc.* 13^{th} *Int. Conf. Nuclear Engg., Beijing, China*, 16-20.